

Drone-Based Antenna Beam Calibration in the High Arctic

LAWRENCE HERMAN¹, CHRISTOPHER BARBARIE¹, MOHAN AGRAWAL¹, VLAD CALINESCU¹, SIMON CHEN¹, H. CYNTHIA CHIANG¹, CHERIE K. DAY¹, EAMON EGAN¹, STEPHEN FAY¹, KIT GERODIAS¹, MAYA GOSS¹, MICHAEL HÉTU¹, DANIEL C. JACOBS², MARC-OLIVIER R. LALONDE^{1,2}, FRANCIS MCGEE¹, LOÏC MIARA¹, JOHN ORLOWSKI-SCHERER^{1,3}, AND JONATHAN SIEVERS¹

¹Department of Physics, McGill University, Montréal, QC, H3A 2T8, Canada

²School of Earth and Space Exploration, Arizona State University, Tempe, AZ, 85287, USA

³Department of Physics and Astronomy, University of Pennsylvania, Philadelphia, PA, 19104, USA

CORRESPONDING AUTHOR: Lawrence Herman (e-mail: lawrence.herman@mail.mcgill.ca).

ABSTRACT The development of low-frequency radio astronomy experiments for detecting 21-cm line emission from hydrogen presents new opportunities for creative solutions to the challenge of characterizing an antenna beam pattern. The Array of Long Baseline Antennas for Taking Radio Observations from the Seventy-ninth parallel (ALBATROS) is a new radio interferometer sited in the Canadian high Arctic that aims to map Galactic foregrounds at frequencies below ~ 30 MHz. We present PteroSoar, a custom-built hexacopter outfitted with a transmitter, that will be used to characterize the beam patterns of ALBATROS and other experiments. The PteroSoar drone hardware is motivated by the need for user-servicing at remote sites and environmental factors that are unique to the high Arctic. In particular, magnetic heading is unreliable because the magnetic field lines near the north pole are almost vertical. We therefore implement moving baseline real time kinematic (RTK) positioning with two GPS units to obtain heading solutions with $\sim 1^\circ$ accuracy. We present a preliminary beam map of an ALBATROS antenna, thus demonstrating successful PteroSoar operation in the high Arctic.

INDEX TERMS drone, radio astronomy, calibration, Arctic

I. INTRODUCTION

CALIBRATING receivers used in radio astronomy experiments requires accurate measurements of the on-sky spatial response, or beam pattern. For experiments that employ dishes or antennas with active drive systems, beam measurements are typically obtained by scanning the instrument across bright celestial sources. This method is not possible for experiments with stationary antennas. Some experiments have successfully used source transits to obtain one-dimensional beam profiles, which can be combined to yield two-dimensional maps [1]–[4]. However, as any individual celestial source transits only once per day, this measurement process necessarily takes place on long time scales. To characterize beam patterns of stationary antennas on shorter time scales, one solution is to employ a drone that flies a transmitting source relative to the instrument. Drone-based calibration systems for radio astronomy, using a variety of designs and instrumental approaches, have been successfully demonstrated in the literature [5]–[11].

We present the PteroSoar system, a new drone-based calibrator that operates in the high Arctic and therefore has unique design considerations. One experimental use-case of PteroSoar is the Array of Long Baseline Antennas for Taking Radio Observations from the Seventy-ninth parallel (ALBATROS, [12]). ALBATROS aims to map Galactic foregrounds at $\lesssim 30$ MHz with improved resolution relative to existing measurements. These maps will lay the groundwork for future measurements of the cosmic dark ages. ALBATROS is sited at the McGill Arctic Research Station (MARS) [13], which is located on Axel Heiberg Island, Nunavut, in the Canadian high Arctic (Figure 1). In this paper, we describe the design of the PteroSoar drone and transmitting payload, beam mapping flight operations, and preliminary ALBATROS beam mapping results from the 2023 Arctic summer.



FIGURE 1. PteroSoar in flight over an ALBATROS station located on Axel Heiberg Island at MARS. The station includes an antenna (background) located 30 m from the readout and power systems (foreground).

II. The PteroSoar System Design

A. Drone

The PteroSoar drone is a custom-built hexacopter (Figure 2). A customized rather than off-the-shelf solution offers several advantages, chief among them cost. Beam mapping operations require long flight times with payloads that are typically $\gtrsim 1$ kg. Few commercial drones are optimized for this kind of operation, and they typically cost $\gtrsim \$15K$. This high cost presents a significant risk for remote Arctic operations, where flyaways or similarly catastrophic events can easily result in complete drone loss. The ability to service and repair components is another advantage of a custom build. Many commercial systems are not user-serviceable, and any subsystem failures at a remote deployment site would result in hard termination of drone operations.

The PteroSoar drone design (Figure 3) is based largely off of the External Calibrator for Hydrogen Observatories [7] and uses mostly hobbyist, off-the-shelf components. The drone employs a Tarot Iron Man 680 carbon fiber frame for a high strength-to-weight ratio with overall dimensions $1015 \text{ mm} \times 1015 \text{ mm} \times 330 \text{ mm}$. Power is supplied by a single 6S lithium-polymer 17000 mAh battery from Tattu. One battery at a time is used for flight and provides approximately 30 minutes of flight time at an altitude of 200 ft above ground level (AGL). The weight of the drone alone, including the battery but excluding the payload, is approximately 4 kg. The motors, propellers, and electronic speed controllers (ESCs) are from the DJI E800 kit. Each motor is capable of supplying 2100 g of thrust. Considering this maximum thrust rating, to maintain a 2:1 thrust-to-

weight ratio, the maximum payload the drone can carry is approximately 2.5 kg. A Pixhawk Cube Orange flight controller, mounted on the drone frame central platform, commands the ESCs to set the drone's attitude and motion. The drone can accept either a pre-programmed flight path from the flight controller or manual navigation. The flight controller also contains a barometric sensor for altitude estimation and three orthogonal accelerometers/gyroscopes for attitude and motion sensing. Telemetry is streamed to a laptop base station via a 915-MHz, 100-mW radio link. Open-source software from QGroundControl¹ is used for flight planning, control of the drone, and setting the drone's various software parameters. A FrSky Taranis X9D Plus SE 2019 handheld controller provides manual control of the drone over a 2.4-GHz, 32-mW radio link. The flight control rules and parameters of the drone are configurable. Typically, while manually flying the drone, roll and pitch are controlled via acceleration command and yaw via rate command. Position estimation and heading input are provided via a dual-GPS system (to be discussed further in §IV) using Holybro F9P Helical GNSS modules. PteroSoar is certified by Transport Canada as meeting the requirements for flight in controlled airspace.

B. Calibrator Payload

The design of the PteroSoar calibrator payload is shown in Figure 4. The transmitted radio signal is generated by a Leo Bodnar mini precision GPS reference clock. This clock

¹<https://qgroundcontrol.com/>



FIGURE 2. The PteroSoar drone in flight, equipped with the transmitting payload.

source is tunable from 400 Hz to 810 MHz via software; to date, we have performed measurements at 50 MHz. The output signal strength is approximately 10 dBm, which is sufficient for ALBATROS measurements at 50 MHz without additional amplification. The Leo Bodnar output signal is passed to an HMC545 RF switch and is modulated at 10 Hz against a 50-Ω terminator. This modulation facilitates separation of the calibration signal from background noise in post-processing, and the chopping frequency is chosen to be compatible with the flight speed and data acquisition rates (further details in §III). The modulation is controlled by an Arduino Mega. The modulated signal at the output of the RF switch is passed to an Aaronia BicoLOG 5070 antenna. We selected the Aaronia antenna for the initial PteroSoar demonstration because the hardware is commercially available and well characterized. Future measurements for ALBATROS

will require a different antenna that is optimized for lower frequencies. All of the calibrator payload components are powered with a 5-V USB power bank. A custom 3D-printed mounting system houses the payload components and secures them against the drone frame. In the event of a hard landing, the 3D-printed mount is designed to break away from the frame to minimize damage to the drone and the payload. The total weight of the payload is approximately 1 kg.

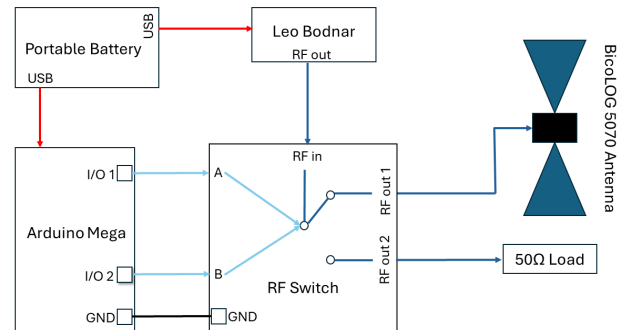


FIGURE 4. Block diagram of the transmitter payload. The 5-V portable battery powers all active components, as indicated by the red arrows. The Leo Bodnar produces the transmitted RF signal which is passed to the RF switch, with the RF signal paths shown in blue. The Arduino Mega controls the RF switch via logic circuitry (cyan arrows), which alternates between a 50 Ω terminator and the BicoLOG 5070 antenna.

III. Flight Path Planning

A. Overview

The PteroSoar standard operating procedure is to fly automated patterns over the antenna under test (AUT) when performing beam measurements, although manual control of the drone is also possible. Flights are continuously monitored from the laptop base station, which receives telemetry from the drone. Considerations that influence the automated flight path planning include:

- Altitude corresponding to the far field of the AUT
- Required beam map coverage and resolution
- Battery life
- Transmitter chopping frequency
- Drone timestamping frequency
- AUT readout system data rate

This section discusses flight pattern determination for measuring the AUT main beam, using the ALBATROS antenna and operating parameters as a case study. The analysis is similar when planning flight profiles for beam sidelobes and other types of measurements.

B. Flight Altitude and Area Coverage

Desired flight altitude and area coverage determine most of the parameters of the drone's automated pattern. For the ALBATROS tests presented here, we map a portion of the

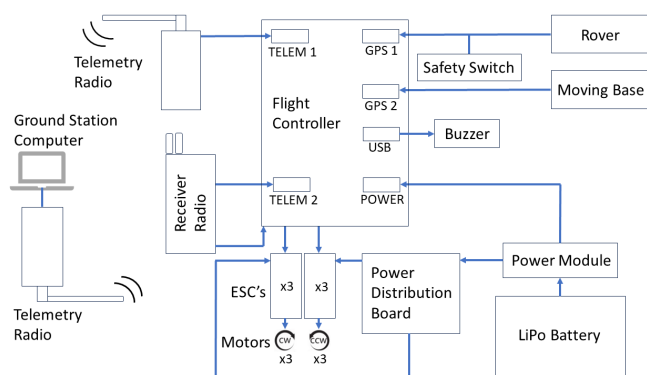


FIGURE 3. Block diagram of drone components. The drone is controlled by a Pixhawk Cube Orange flight controller. The flight controller is equipped with multiple sensors for determining attitude. The Cube Orange takes input from the dual GPS system (rover and moving base), the telemetry radios, and the receiver radio. The electronic speed controllers (ESCs), which are connected to the motors, are commanded by the flight controller. The entire system is powered by a lithium polymer battery.

main beam spanning approximately $80^\circ \times 80^\circ$. The far-field distance of the AUT dictates the flight altitude. At a frequency of 50 MHz, corresponding to a wavelength of approximately 6 m, the 2-m diameter ALBATROS antenna falls between electrically short and resonant. The far-field distances for these two cases are 2λ and $2D^2/\lambda$, respectively, where λ is the wavelength and D is the diameter. These expressions yield a maximum far-field distance of 12 m for ALBATROS at 50 MHz. We choose a flight altitude of 60 m AGL to place the drone well in the far field, while staying within legal restrictions and limiting battery power consumption from ascending/descending. In Canada, the maximum legal altitude for drone flight is 122 m AGL without special permission from Transport Canada. Testing revealed that ascent to and descent from 122 m AGL depletes approximately 20% of the drone battery. At 60 m altitude, $80^\circ \times 80^\circ$ beam coverage corresponds to linear dimensions of approximately 100 m \times 100 m.

C. Row Spacing and Flight Speed

The drone flies a raster pattern at fixed altitude to fill the required beam mapping area. For the ALBATROS main beam, we select a beam map resolution of 1° , which corresponds to ~ 1 m linear distance at 60 m altitude. The row spacing of the raster pattern is set to this distance. The flight speed is determined by competing requirements that are set by various timestream rates and the drone battery life. The PteroSoar transmitter is chopped at 10 Hz, and the position timestamps are also logged at 10 Hz. The drone therefore cannot exceed a flight speed of $(1 \text{ m})/(0.1 \text{ sec}) = 10 \text{ m/s}$ to meet the 1° beam map resolution requirement. The ALBATROS readout system digitizes the antenna timestreams at 250 Msps and saves channelized, 4-bit data at 50 MHz every $16.384 \mu\text{s}$. Because this data rate is much greater than the transmitter chopping and position timestamp frequencies, the ALBATROS readout system does not constrain the drone flight speed. The minimum flight speed is set by the battery life, which is ~ 30 minutes per flight, and the number of batteries that are available to swap during the measurement. For ALBATROS, we set the flight speed to approximately 1.5 m/s, which yields a high density of measurement points for demodulation (§V) and ensures that the beam map resolution requirement is satisfied. A complete beam map measurement requires roughly two fully charged batteries.

IV. Arctic Challenges

A. Arctic 2022–2023 Overview

Drone operations in the Arctic have unique challenges associated with the remote location and polar latitudes. Our initial attempts at Arctic flying in 2022 were stymied by unexpected heading sensor anomalies. After implementing a new GPS-based heading system, further operations in 2023 were ultimately successful, after overcoming additional challenges in diagnosing, repairing, and preventing vibration-induced flight errors in this isolated environment.

B. Magnetometer

Initial attempts to fly the drone at MARS in 2022 were unsuccessful; the drone flight behavior became erratic immediately following take-off, resulting in crashes. A software extended Kalman filter in the Cube Orange Pixhawk flight controller processes various sensor inputs into state estimations, including drone position, altitude, attitude, and heading. The magnetometer is typically the primary source of yaw angle information. To determine the validity of the magnetometer signal, the flight controller computes an innovation test ratio. The magnetometer innovation is the difference between the measured and forecasted values, and the test ratio compares the innovation against the three-standard-deviation scatter of the measured signal. Under normal operation, the innovation test ratio should stay below 0.5; however, the ratio significantly exceeded unity in the initial 2022 flight attempts. The poor signal quality was caused by the magnetic inclination at MARS, which is $\sim 88^\circ$. Because the Earth's magnetic field is only $\sim 2^\circ$ off vertical, the magnetometer was unable to obtain reliable yaw or heading information for the Kalman filter, thus resulting in uncontrollable flight.

C. Dual GPS Solution

To bypass the unreliable magnetometer readings, a GPS-based heading solution using dual receivers was implemented for MARS flights in 2023. Each receiver is mounted at an extended distance from the drone body, forming a back-to-front baseline separation of ~ 66 cm. Moving base real time kinematics (RTK) enables the dual-GPS system to supply heading information, using a vector from the rear “moving base” unit to the front “rover” unit (Figure 3). The GPS units can be installed with a different baseline orientation angle, provided that the offset is passed to the flight controller software. The receivers used in the PteroSoar dual-GPS system are Holybro F9P Helical units that incorporate u-blox ZED-F9P modules. Released in 2019, the u-blox ZED-F9P module is capable of multi-band reception for centimeter-level accuracy. The PteroSoar dual-GPS system thus achieves a heading accuracy of $\sim 1^\circ$ using a receiver baseline separation that fits comfortably within the drone footprint.

D. Mitigating Flight Controller Vibration

The Arctic 2023 flight campaign was further complicated by excessive flight controller vibrations, which were not present in previous PteroSoar test flights. The unexpected vibrations caused two crashes in rapid succession, which significantly damaged the drone. Despite the setbacks, the custom-built architecture of PteroSoar enabled successful on-site repairs in the Arctic, where the selection of spare parts and raw materials is highly limited. The on-site repairs included removing and reattaching a motor arm, replacing the landing skids, and replacing broken mounting hardware.

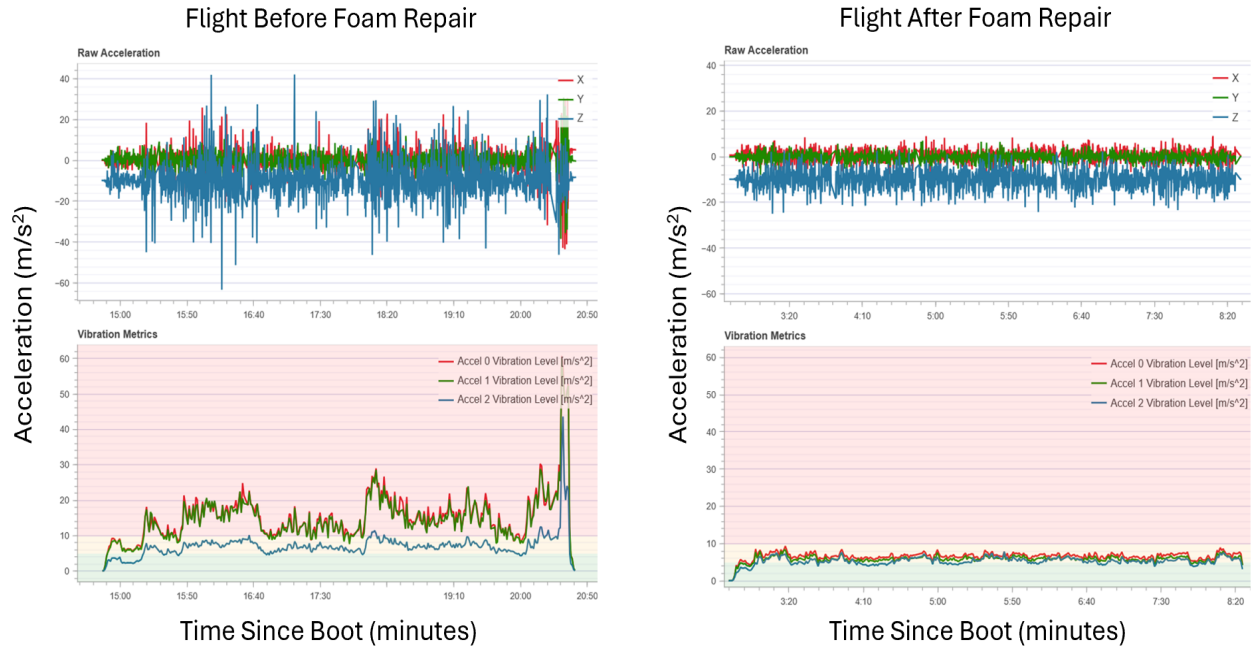


FIGURE 5. The raw acceleration and vibration metrics prior to (left) and after (right) implementing the vibration mitigation strategy. Under normal operation, the raw acceleration should have X and Y components that are both near zero, and the Z component should be close to $-1g$ for level flight. The green and yellow regions in the vibration metrics plots indicate acceptable values for stable flight, and extended excursions into the red region typically cause flight controller faults and subsequent crashes.

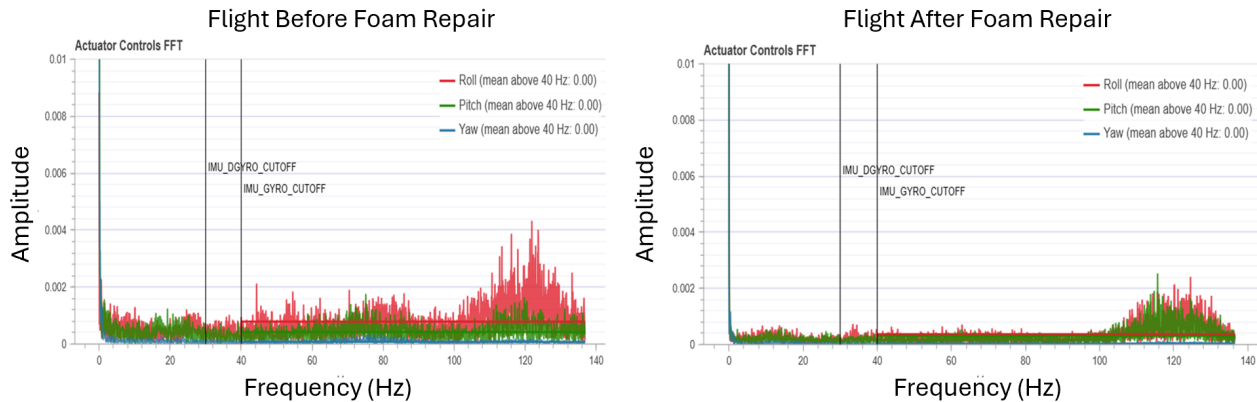


FIGURE 6. The actuator controls FFT prior to (left) and after (right) implementing the vibration mitigation strategy. The black vertical lines indicate the cutoff frequencies for the angular acceleration (DGYRO) and the low-pass filter cutoff (GYRO), which are set to their default values in the Pixhawk firmware. Under normal operation, the actuator controls FFT should have a single peak below 20 Hz and should be flat up to ~ 100 Hz.

Analysis of the drone log files isolated the cause of the crashes to excessive vibrations resulting in Kalman filter faults. The left panels of Figure 5 show the abnormal readings of “raw acceleration” and “vibration metrics” data from the open-source Pixhawk flight controller logs. Raw acceleration data come directly from the flight controller’s accelerometers in each axis. Under normal operation, the lateral X and Y components should remain close to zero relative to Earth’s gravity ($g = 9.8 \text{ m/s}^2$), and the vertical Z component should be roughly $-1g$ in level flight. Vibration metrics are a low-pass filtered measurement of vibration data, and the green and yellow regions indicate acceptable levels

for stable flight operations. The left panel of Figure 6 shows the “actuator controls FFT” reported by the Pixhawk, which provides spectral amplitudes of the actuator control signals for the roll, pitch, and yaw axes. Under normal operation, the amplitudes should be flat over most of the frequency range, indicating smooth and controlled actuator inputs and stable flight.

To mitigate the flight controller vibrations, a piece of semi-rigid foam was placed between the flight controller and the drone’s frame. Several types of foam were tested before deciding on an acceptable solution. The right panels of Figures 5 and 6 show that the raw acceleration, vibration

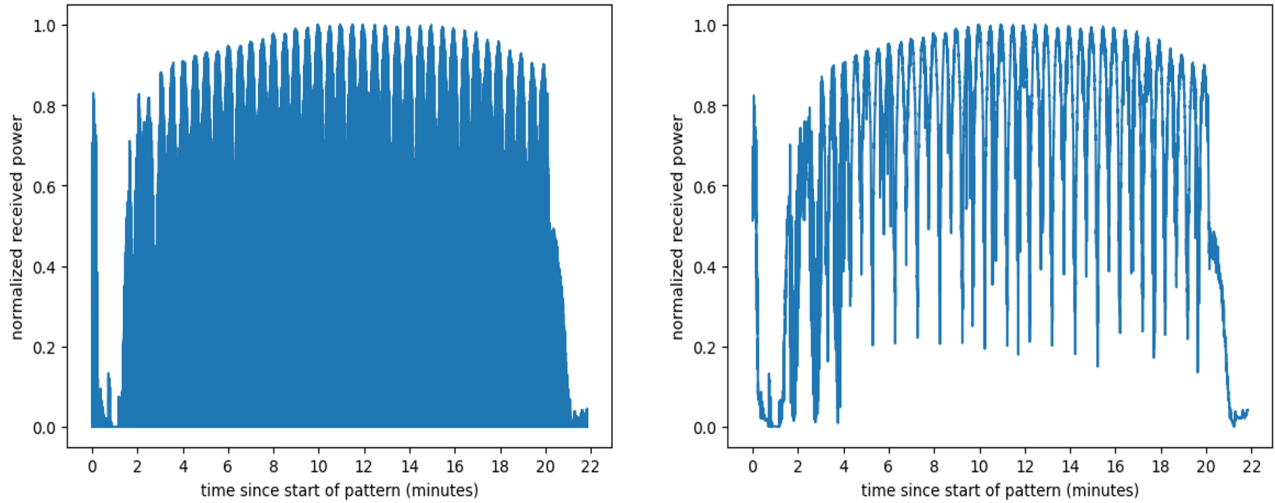


FIGURE 7. Raw (left) and demodulated (right) ALBATROS timestream data from a drone beam mapping flight conducted at MARS during 2023. The background noise at MARS is effectively zero, so the demodulated data are essentially the envelope of the raw data.

metrics, and actuator controls FFT all lie within acceptable ranges following the foam repair. After installing the foam, PteroSoar flew for 36 sorties totalling over 8 flight hours without further incident.

V. Data Processing and Initial Results

We average blocks of 500 ALBATROS baseband spectra to create power data with ~ 8 ms time resolution. The averaged baseband data are fit with a square wave to capture the 10-Hz chopped signal from the drone-mounted transmitter. Within each contiguous segment corresponding to periods when the transmitter is on or off, the time-ordered data are averaged together, and data points falling in the on-off transitions are cut. From each “on” period, we subtract the average of the neighboring “off” periods to remove background noise and self-generated radio-frequency interference. The timestamp for each background-subtracted measurement is calculated using the write rate of the readout system, referenced to the starting time of the data file.

The flight controller’s open-source log files provide drone position data and timestamps. The local position from fused sensor data of the drone’s inertial measurement units, GPSs, and barometer are saved in local north, east, and down coordinates in units of meters. These data are converted to spherical coordinates for subsequent analysis. The native timestamps are referenced to the system boot-up time and are converted to Unix time in post-processing. Each drone position timestamp is used to interpolate baseband data and assign a measured signal value to every drone coordinate. The interpolated baseband data are binned into a Healpix [14] map with $n_{side} = 32$, corresponding to 1.8° pixels.

Figure 7 shows the pre- and post-demodulated timestream data (left and right panels, respectively) from a mapping flight conducted over the central ALBATROS station near the

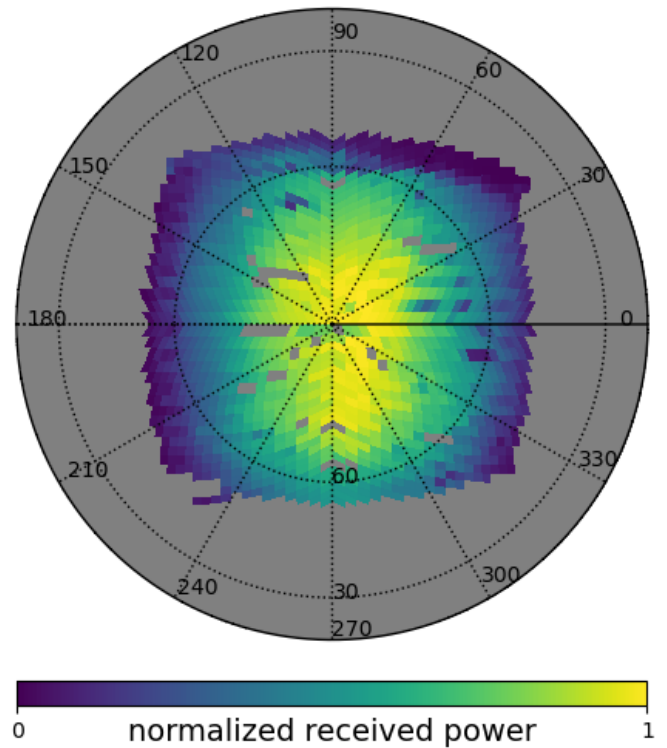


FIGURE 8. Preliminary map of received power by the ALBATROS antenna in normalized baseband units, without systematic error corrections. This map shows binned data for a single polarization from the ALBATROS crossed dipole. The polarization of the drone transmitter was aligned with the dipole axis during flight.

MARS main camp. Compared to the drone-mounted radio source, the background noise level at MARS is effectively zero. Consequently, the demodulated timestream data are effectively the envelope of the raw data. The time-ordered data show a visible rise and fall in the signal level as the drone approaches and recedes from the antenna in flight. The demodulated timestream is interpolated and merged with drone position data, and the resulting binned beam map is shown in Figure 8. This map shows a single polarization from the ALBATROS crossed dipole. Corrections for systematic effects have not been applied at this time and will be addressed in a future publication. The polarization of the drone transmitter was aligned with the dipole axis during flight, thus yielding a qualitative measurement of the copolar main beam.

VI. Lessons Learned and Future Work

We have demonstrated successful initial beam mapping operations in the high Arctic with the PteroSoar drone calibration system. The custom-built architecture has enabled on-site optimization, modifications, and repair work that would otherwise be difficult or impossible with commercial, off-the-shelf systems that are not designed to be serviced by the user. However, using a custom-built system also requires increased discipline in pre-flight checks (e.g., checking for connections that loosen with time from vibrations) and careful monitoring of the flight logs for any unexpected changes.

We will continue drone beam mapping flights for ALBATROS in the high Arctic as we build up the array in the coming years. With the initial proof-of-concept in hand, our focus will turn toward more complete mapping efforts of the main beam and sidelobes for all antennas in the array. Our plan of work includes redesigning the transmitter payload to target lower frequencies corresponding to the ALBATROS primary science goals. We are investigating new motors, speed controllers, flight controllers, and batteries to further improve the PteroSoar drone performance. We are additionally developing a remotely controlled implementation of the signal chopper, which will improve flight efficiency by eliminating the need to land the drone for changing the chopper settings. Our future measurement plans also include investigating systematic effects associated with the drone and the transmitter so that we can work toward beam maps that have sufficient accuracy for science analyses.

ACKNOWLEDGMENTS

We gratefully acknowledge the Natural Sciences and Engineering Research Council of Canada (RGPIN-2019-04506, RGPNS-2019-534549), the Canada Foundation for Innovation John R. Evans Leaders Fund (40824), the New Frontiers in Research Fund (NFRFE-2021-00409), the National Geographic Society (NGS-949383T-22), and the Polar Continental Shelf Program (PCSP) for providing funding and logistical support for our research program. This research was undertaken, in part, thanks to funding from the

Canada 150 Program. This research was enabled in part by support provided by the Digital Research Alliance of Canada (alliancecan.ca). We extend our sincere gratitude to the PCSP Resolute staff for their generous assistance and bottomless cookie jars. The authors thank Chris Omelon, Laura Thomson, Anthony Zerafa, Olivia Locke, and all of the MARS researchers for their invaluable advice and field help.

REFERENCES

- [1] M. Amiri, K. Bandura, A. Boskovic, J.-F. Cliche, M. Deng, M. Dobbs, M. Fandino, S. Foreman, M. Halpern, A. S. Hill, G. Hinshaw, C. Höfer, J. Kania, T. L. Landecker, J. MacEachern, K. Masui, J. Mena-Parra, L. Newburgh, A. Ordog, T. Pinsonneault-Marotte, A. Polzin, A. Reda, J. R. Shaw, S. R. Siegel, S. Singh, K. Vanderlinde, H. Wang, J. S. Willis, D. Wulf, and CHIME Collaboration, "Using the Sun to Measure the Primary Beam Response of the Canadian Hydrogen Intensity Mapping Experiment," *The Astrophysical Journal*, vol. 932, no. 2, p. 100, Jun. 2022.
- [2] A. Chokshi, J. L. B. Line, N. Barry, D. Ung, D. Kenney, A. McPhail, A. Williams, and R. L. Webster, "Dual polarization measurements of MWA beampatterns at 137 MHz," *Monthly Notices of the Royal Astronomical Society*, vol. 502, no. 2, pp. 1990–2004, 01 2021. [Online]. Available: <https://doi.org/10.1093/mnras/stab156>
- [3] J. L. B. Line, B. McKinley, J. Rasti, M. Bhardwaj, R. B. Wayth, R. L. Webster, D. Ung, D. Emrich, L. Horsley, A. Beardsley, B. Crosse, T. M. O. Franzen, B. M. Gaensler, M. Johnston-Hollitt, D. L. Kaplan, D. Kenney, M. F. Morales, D. Pallot, K. Steele, S. J. Tingay, C. M. Trott, M. Walker, A. Williams, and C. Wu, "In situ measurement of MWA primary beam variation using ORBCOMM," *Publications of the Astronomical Society of Australia*, vol. 35, p. e045, Dec. 2018.
- [4] A. R. Neben, R. F. Bradley, J. N. Hewitt, G. Bernardi, J. D. Bowman, F. Briggs, R. J. Cappallo, A. A. Deshpande, R. Goetze, L. J. Greenhill, B. J. Hazelton, M. Johnston-Hollitt, D. L. Kaplan, C. J. Lonsdale, S. R. McWhirter, D. A. Mitchell, M. F. Morales, E. Morgan, D. Oberoi, S. M. Ord, T. Prabu, N. U. Shankar, S. S. Srivani, R. Subrahmanyam, S. J. Tingay, R. B. Wayth, R. L. Webster, A. Williams, and C. L. Williams, "Measuring phased-array antenna beampatterns with high dynamic range for the Murchison Widefield Array using 137 MHz ORBCOMM satellites," *Radio Science*, vol. 50, no. 7, pp. 614–629, Jul. 2015.
- [5] K. Bhopi, W. Tyndall, P. Sanghavi, K. Bandura, L. Newburgh, and J. Gallicchio, "A Digital Calibration Source for 21 cm Cosmology Telescopes," *Journal of Astronomical Instrumentation*, vol. 11, no. 4, p. 2250016, Jan. 2022.
- [6] K. P. Makhija, V. Sukhil, B. D. Nhan, J. B. Dugan, and R. F. Bradley, "The Precision Radio Instrument for Antenna Measurements (PRIAM): measurement strategy," in *2021 XXXIVth General Assembly and Scientific Symposium of the International Union of Radio Science (URSI GASS)*, 2021, pp. 1–4.
- [7] D. C. Jacobs, J. Burba, J. D. Bowman, A. R. Neben, B. Stinnett, L. Turner, K. Johnson, M. Busch, J. Allison, M. Leatham, V. Serrano Rodriguez, M. Denney, and D. Nelson, "First Demonstration of ECHO: an External Calibrator for Hydrogen Observatories," *Publications of the Astronomical Society of the Pacific*, vol. 129, no. 973, p. 035002, Mar. 2017.
- [8] P. Bolli, F. Paonessa, G. Pupillo, G. Virone, M. Arts, A. Lingua, J. Monari, and S. J. Wijnholds, "Antenna pattern characterization of the low-frequency receptor of LOFAR by means of an UAV-mounted artificial test source," in *Ground-based and Airborne Telescopes VI*, ser. Society of Photo-Optical Instrumentation Engineers (SPIE) Conference Series, H. J. Hall, R. Gilmozzi, and H. K. Marshall, Eds., vol. 9906, Jul. 2016, p. 99063V.
- [9] C. Chang, C. Monstein, A. Refregier, A. Amara, A. Glauser, and S. Casura, "Beam Calibration of Radio Telescopes with Drones," *Publications of the Astronomical Society of the Pacific*, vol. 127, no. 957, p. 1131, Nov. 2015.
- [10] G. Pupillo, G. Naldi, G. Bianchi, A. Mattana, J. Monari, F. Perini, M. Poloni, M. Schiaffino, P. Bolli, A. Lingua, I. Aicardi, H. Bendea, P. Maschio, M. Piras, G. Virone, F. Paonessa, Z. Farooqui, A. Tibaldi,

- G. Addamo, O. A. Peverini, R. Tascone, and S. J. Wijnholds, "Medicina array demonstrator: calibration and radiation pattern characterization using a UAV-mounted radio-frequency source," *Experimental Astronomy*, vol. 39, no. 2, pp. 405–421, Jun. 2015.
- [11] G. Virone, A. M. Lingua, M. Piras, A. Cina, F. Perini, J. Monari, F. Paonessa, O. A. Peverini, G. Addamo, and R. Tascone, "Antenna Pattern Verification System Based on a Micro Unmanned Aerial Vehicle (UAV)," *IEEE Antennas and Wireless Propagation Letters*, vol. 13, pp. 169–172, Jan. 2014.
- [12] H. C. Chiang, T. Dyson, E. Egan, S. Eyono, N. Ghazi, J. Hickish, J. M. Jáuregui-García, V. Manukha, T. Ménard, T. Moso, J. Peterson, L. Philip, J. L. Sievers, and S. Tartakovsky, "The Array of Long Baseline Antennas for Taking Radio Observations from the Sub-Antarctic," *Journal of Astronomical Instrumentation*, vol. 9, no. 4, pp. 2 050 019–564, Jan. 2020.
- [13] T. Dyson, H. C. Chiang, E. Egan, N. Ghazi, T. Ménard, R. A. Monsalve, T. Moso, J. Peterson, J. L. Sievers, and S. Tartakovsky, "Radio-Frequency Interference at the McGill Arctic Research Station," *Journal of Astronomical Instrumentation*, vol. 10, no. 2, pp. 2 150 007–564, Jan. 2021.
- [14] K. M. Górski, E. Hivon, A. J. Banday, B. D. Wandelt, F. K. Hansen, M. Reinecke, and M. Bartelmann, "HEALPix: A Framework for High-Resolution Discretization and Fast Analysis of Data Distributed on the Sphere," *The Astrophysical Journal*, vol. 622, no. 2, pp. 759–771, Apr. 2005.